ADVANCED FUNCTIONAL MATERIALS
www.afm-journal.de

www.MaterialsViews.com

Biocompatible, Uniform, and Redispersible Mesoporous Silica Nanoparticles for Cancer-Targeted Drug Delivery In Vivo

Quan Zhang, Xiaoling Wang, Pei-Zhou Li, Kim Truc Nguyen, Xiao-Jun Wang, Zhong Luo, Huacheng Zhang, Nguan Soon Tan, and Yanli Zhao**

Engineering multifunctional nanocarriers for targeted drug delivery shows promising potentials to revolutionize the cancer chemotherapy. Simple methods to optimize physicochemical characteristics and surface composition of the drug nanocarriers need to be developed in order to tackle major challenges for smooth translation of suitable nanocarriers to clinical applications. Here, rational development and utilization of multifunctional mesoporous silica nanoparticles (MSNPs) for targeting MDA-MB-231 xenograft model breast cancer in vivo are reported. Uniform and redispersible poly(ethylene glycol)-incorporated MSNPs with three different sizes (48, 72, 100 nm) are synthesized. They are then functionalized with amino-β-cyclodextrin bridged by cleavable disulfide bonds, where amino-β-cyclodextrin blocks drugs inside the mesopores. The incorporation of active folate targeting ligand onto 48 nm of multifunctional MSNPs (PEG-MSNPs48-CD-PEG-FA) leads to improved and selective uptake of the nanoparticles into tumor. Targeted drug delivery capability of PEG-MSNPs48-CD-PEG-FA is demonstrated by significant inhibition of the tumor growth in mice treated with doxorubicin-loaded nanoparticles, where doxorubicin is released triggered by intracellular acidic pH and glutathione. Doxorubicin-loaded PEG-MSNPs48-CD-PEG-FA exhibits better in vivo therapeutic efficacy as compared with free doxorubicin and non-targeted nanoparticles. Current study presents successful utilization of multifunctional MSNP-based drug nanocarriers for targeted cancer therapy in vivo.

1. Introduction

The advantages of nanocarriers in targeted drug delivery include the minimization of nonspecific toxicity and the enhancement of therapeutic efficiency when compared with conventional small-molecule chemotherapy.[1–5] Recent studies have demonstrated successful cancer-targeted delivery of drugs encapsulated within various nanomaterials, including liposomes,[6–9] polymeric nanoparticles,[10,11] dendrimers,[12] and inorganic-organic hybrid nanoparticles.[13–16] Considering their large surface-to-volume ratio, nanocarriers offer the possibility of transporting large quantities of anti-cancer drugs to tumor tissues. On the other hand, passive and active targeting effects limit harmful systemic distribution. Passive targeting strategies rely on the enhanced permeation and retention (EPR) effects to direct the accumulation of nanocarriers at tumor sites.[17,18] However, the lack of cell-specific interactions for the internalization of nanocarriers decreases therapeutic efficacy, resulting in the drug expulsion and the induction of multiple drug resistance.[19,20] In order to further enhance selective targeting ability of nanocarriers towards cancer cells, grafting the targeting units, such as antibodies and folic acid, onto the nanocarrier surfaces allows active targeting, thus reducing the side effects by decreasing their interactions with healthy cells.[2,21–23]

Traditional drug carriers suffer from unexpected drug release during the circulation. Ideal drug carriers should be able to encapsulate drugs efficiently before reaching tumor sites. In this regard, mesoporous silica nanoparticles (MSNPs) as drug carriers possess unique advantages including stable mesoporous structure, large surface area, and tunable pore size, which are favorable for the drug

Dr. Q. Zhang, Dr. P.-Z. Li, K. T. Nguyen, Dr. X.-J. Wang, Dr. Z. Luo, Dr. H. Zhang, Prof. Y. L. Zhao
Division of Chemistry and Biological Chemistry
School of Physical and Mathematical Sciences
Nanyang Technological University
21 Nanyang Link, Singapore, 637371
E-mail: zhaoyanli@ntu.edu.sg
Dr. X. Wang, Prof. N. S. Tan
School of Biological Sciences
Nanyang Technological University
60 Nanyang Drive, Singapore, 637551
E-mail: nstan@ntu.edu.sg

DOI: 10.1002/adfm.201302988

Dr. Q. Zhang
Key Laboratory of Carbohydrate Chemistry and Biotechnology, Ministry of Education
School of Biotechnology
Jiangnan University
Lihu Avenue 1800, Wuxi, China, 214122
Prof. Y. L. Zhao
School of Materials Science and Engineering
Nanyang Technological University
50 Nanyang Avenue, Singapore, 639798
Prof. N. S. Tan
Institute of Molecular and Cell Biology
A*STAR, 61 Biopolis Drive, Singapore, 138673

© 2013 WILEY-VCH Verlag GmbH & Co. KGaA, Weinheim

loading.[24–29] Most researches on MSNP-based drug carriers focused on the encapsulation of anticancer drugs within the nanopores followed by closing the pore entrances with different caps.[30–39] Upon appropriate stimulation, the caps are either opened or removed, and the cargos in the reservoir are released into a specific environment. For example, cyclodextrin (CD) gated MSNPs can efficiently store different cargos within the pores and be triggered to release the loaded cargos in response to external stimuli such as changes in redox state[40–42] and pH,[43–45] enzyme actions,[46,47] and photoirradiation.[48,49] However, most of the abovementioned systems were evaluated in solution and/or in vitro, and their in vivo capabilities remained unclear. Although significant advancements have been achieved with these stimulus-triggered drug release systems, it is still a challenge to simultaneously realize high targeting specificity and controlled drug release, while avoiding non-specific binding and entrapment through the defence of the bodies. For in vivo applications, MSNP-based drug carriers should meet the following prerequisites: i) high stability in physiologically relevant conditions,[50–52] ii) sizes of 10–100 nm in diameter to prevent rapid elimination from the blood through kidney and liver,[53,54] iii) sufficient targeting ligands on the surface of the nanoparticle carriers to maximize their uptake in cancer cells while minimizing non-specific uptake in off-target cells, and iv) being capable of eliminating undesired drug release before reaching tumor, and releasing drugs specifically to provide an effective dose inside the cancer cells.

Recently, we have developed a new class of multifunctional MSNP-based systems to deliver anticancer drugs to specific cancer cells in a targeted and controlled manner.[55] The multifunctional MSNPs have been evaluated in vitro with cooperative effects of specific targeting to cancer cells and stimulus-triggered drug release. Guided by our successful in vitro studies, the objectives of present research were to optimize the size and surface decoration of multifunctional MSNPs with suitable physiochemical properties required for targeting folate receptor (FR) overexpressed cancer cells in vivo. Herein, we report the rational development and utilization of biocompatible, uniform, and redispersible multifunctional MSNPs for cancer-targeted drug delivery in vivo. We also demonstrated significant in vivo therapeutic efficacy of doxorubicin-loaded multifunctional MSNPs with a diameter of 48 nm superior to those of free doxorubicin and non-targeted nanoparticles. Moreover, no obvious sign of toxicity from the drug carriers was observed, because most of multifunctional MSNPs were excreted from the urine and feces of mice after 12 days post-injection.

2. Results and Discussion

2.1. Preparation and Characterization of Multifunctional MSNPs with Different Sizes

Nanoparticles within the sizes of 10–100 nm in diameter are normally desirable. If the nanoparticle sizes are beyond 100 nm, they are too large to be filtered out by kidney, while less than 10 nm, they normally cannot be recognized by reticuloendothelial systems for rapid elimination.[53,54] Common synthetic routes for the preparations of MSNP-based materials result in irreversible nanoparticle aggregation during the surfactant removal and drying processes, and thus obtained large nanoparticle aggregates cannot be homogeneously re-suspended with suitable hydrodynamic sizes.[56] In order to prepare stable suspensions of small MSNPs, Bein and colleagues employed base triethanolamine (TEA) as a substitute of commonly used NaOH or NH_4OH to synthesize MSNPs with diameters of 20–150 nm.[57,58] TEA was considered to act as a complexing agent for silicate species and additionally as a growth inhibitor for mesoporous nanoparticles. However, the final product of this procedure is a gel material of fused nanoparticles, which cannot be re-dispersed during the drying process. In order to prepare small and re-dispersible MSNPs, we further modified Bein's method by increasing the reaction temperature (95 °C) to accelerate the nucleation and by introducing a short-chain poly(ethylene glycol)-silane (PEG-silane, MW 575–750) to terminate the silica condensation on the nanoparticle surface. Thus, PEG-covered MSNPs (PEG-MSNPs) were synthesized via a one-pot reaction in the presence of cetyltrimethylammonium chloride (CTAC) as the template, tetraethylorthosilicate (TEOS) as the silica source, and TEA as the base catalyst (**Figure 1**a).

The transmission electron microscopy (TEM) images shown in **Figure 2** indicate that the size of nanoparticles can effectively be tuned by varying the TEA concentrations and the introduction time of PEG-silane. For example, 4 mg mL^{-1} of TEA with PEG-silane adding time of 10 min afforded 48.3 ± 2.2 nm of PEG-MSNPs (PEG-MSNPs48), 2.5 mg mL^{-1} of TEA and PEG-silane adding time of 20 min resulted in 71.8 ± 3.0 nm of PEG-MSNPs (PEG-MSNPs72), and 1 mg mL^{-1} of TEA and PEG-silane adding time of 30 min achieved 100.2 ± 3.7 nm of PEG-MSNPs (PEG-MSNPs100). Nitrogen adsorption/desorption isotherm measurements show that these PEG-MSNPs possess relatively high specific surface areas of 356.1–655.8 $m^2\ g^{-1}$ with well-defined pore sizes of ≈2.7 nm (Figure S1 in the Supporting Information). Dynamic light scattering (DLS) measurements indicate that these PEG-MSNPs with different sizes could be thoroughly dispersed in phosphate-buffered saline (PBS) solution (pH 7.4) and their hydrodynamic diameters were 61.2 nm (PDI 0.005), 95.4 nm (PDI 0.022), and 123.3 nm (PDI 0.013), respectively (Table S1 in the Supporting Information). In addition, these PEG-MSNPs samples could be dried and re-suspended in PBS without any obvious change in hydrodynamic size (Figure S2 in the Supporting Information), indicating that PEGylated surface modification significantly improves the dispersity of PEG-MSNPs in aqueous solution.

In order to confirm that the CTAC template could be removed from the mesopores of nanoparticles, bare MSNPs without any modifications were prepared and investigated before and after the removal of CTAC using Fourier transform infrared (FT-IR) spectroscopy. Successful CTAC removal was confirmed by complete disappearance of the C–H stretching vibrations between 2928 cm^{-1} and 2853 cm^{-1} and of the C–H bending vibration at 1480 cm^{-1} after the third extraction cycle in a mixture solution of concentrated HCl and ethanol (Figure S3 in the Supporting Information). Next, the functionalizations of different sized PEG-MSNPs were performed according to our previously reported procedure.[55] After the CTAC surfactant template was removed from the nanopores of PEG-MSNPs under acidic conditions, the orifices around the entrances to the nanopores were

© 2013 WILEY-VCH Verlag GmbH & Co. KGaA, Weinheim

ADVANCED FUNCTIONAL MATERIALS
www.afm-journal.de

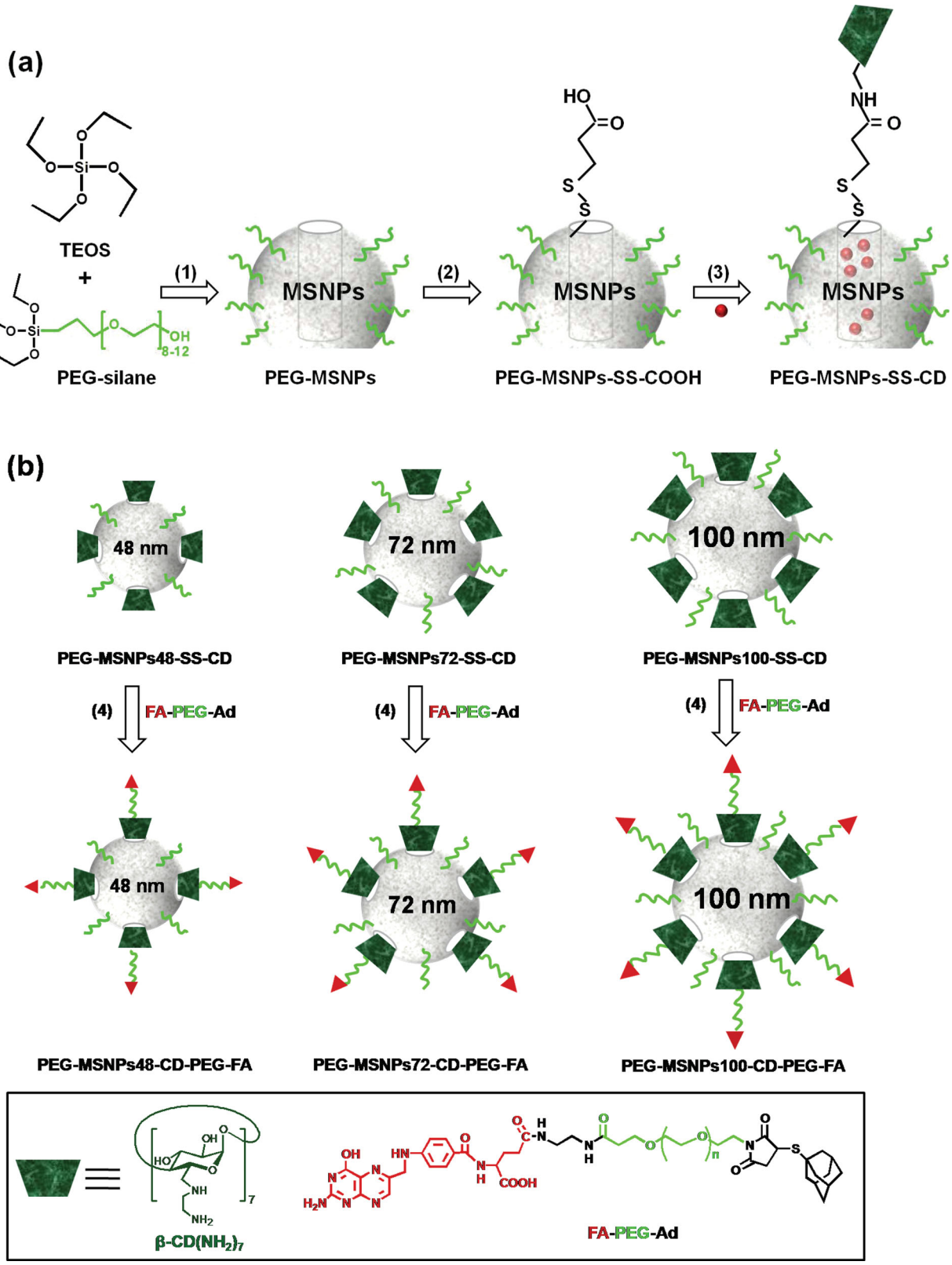

Figure 1. a) Schematic representation of the cargo-loaded PEG-MSNPs-SS-CD. Reaction conditions: 1) triethanolamine in H_2O at 95 °C, followed by the removal of the CTAC template; 2) MPTMS in toluene, followed by the addition of 2-carboxyethyl-2-pyridyl disulfide in ethanol; 3) loading of cargos, followed by the additions of β-CD$(NH_2)_7$ and 1-(3-dimethylaminopropyl)-3-ethylcarbodiimide hydrochloride (EDC·HCl). b) Schematic illustration for preparing PEG-MSNPs-CD-PEG-FA with different nanoparticle sizes of 48, 72, and 100 nm.

© 2013 WILEY-VCH Verlag GmbH & Co. KGaA, Weinheim

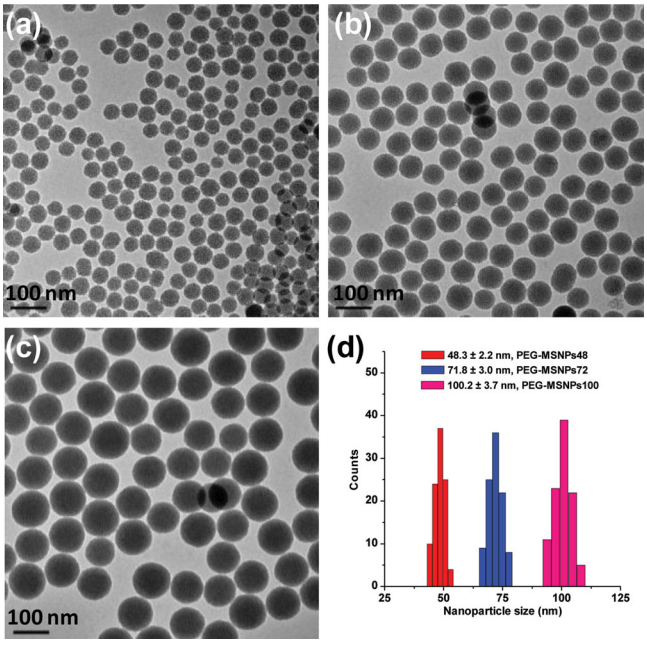

Figure 2. a–c) TEM images of surfactant-free PEG-MSNPs with different sizes: a) PEG-MSNPs48, b) PEG-MSNPs72, and c) PEG-MSNPs100. d) Nanoparticle size distributions of three surfactant-free PEG-MSNPs. The data were calculated from the TEM images.

exposed for modification with mercaptopropyl groups to afford sulphydryl-functionalized nanoparticles, which were further reacted with 2-carboxyethyl-2-pyridyl disulfide to yield carboxylic acid-functionalized nanoparticles (denoted as PEG-MSNPs-SS-COOH, Figure 1a). In order to encapsulate drug molecules (e.g., doxorubicin, Dox) inside the nanopores, the orifices of the nanopores were capped with per-diamino-β-cyclodextrin (β-CD$(NH_2)_7$) via the amidation between carboxylic acid and amino groups, leading to β-CD$(NH_2)_7$ capped MSNPs (denoted as PEG-MSNPs-SS-CD). The fabrication process ensured that the β-CD rings were immobilized selectively around the orifices of the nanopores on the surface of the nanoparticles, as the surface areas between the nanopores on the nanoparticles were covered fully with short PEG chains. Long PEG chains (MW 5000), functionalized with an adamantane (Ad) unit at one end and a folic acid (FA) unit at the other end (denoted as FA-PEG-Ad), were immobilized onto the surface of PEG-MSNPs-SS-CD through strong Ad/β-CD complexation in aqueous solution, offering the FA targeting unit on the surface of the nanoparticles (denoted as PEG-MSNPs-CD-PEG-FA).

To confirm that the FA-PEG-Ad polymers can be immobilized onto PEG-MSNPs-SS-CD via the Ad/β-CD complexation, PEG-MSNPs-SS-CD with different nanoparticle sizes was stirred with FA-PEG-Ad in aqueous solution for 12 h. The nanoparticles coated with FA-PEG-Ad were obtained by centrifugation and washed with H_2O to remove the excess polymers (Figure 1b). TEM images provided direct evidence for the formation of multifunctional MSNPs. When the nanoparticles were incorporated with the β-CD rings followed by the FA-PEG-Ad polymers, the nanoparticle shape did not change significantly, indicating that the nanoparticles retained their morphologies after functionalizations (**Figure 3**a–f). In addition, the nanopore arrays on the nanoparticles cannot be clearly observed after the introduction of the FA-PEG-Ad polymers in aqueous solution, due to the masking of the polymers (Figure 3d–f). DLS measurements show that the hydrodynamic diameters of different-sized PEG-MSNPs-CD-PEG-FA in PBS solution were 72.1 ± 1.6 nm, 107.3 ± 1.4 nm, and 138.9 ± 3.2 nm, respectively (Figure 3g). Larger diameters measured by DLS than those by TEM are attributed to the hydration sphere and outer PEG layer. Based on the DLS measurements, all the polydispersity values of PEG-MSNPs48-CD-PEG-FA (0.013), PEG-MSNPs72-CD-PEG-FA (0.050), and PEG-MSNPs100-CD-PEG-FA (0.053) in PBS were close to zero, indicating good monodispersity of the nanoparticles. The long-term stability of three PEG-MSNPs-CD-PEG-FA samples was evaluated by suspending them in PBS solution (pH 7.4) and cell culture media containing 10% fetal bovine serum (FBS), respectively. No significant size change was observed after incubation for 15 days (Figure 3h), demonstrating their excellent colloidal stability under physiological conditions.

Thermogravimetric analysis (TGA) further confirmed the successful surface functionalization of PEG-MSNPs (**Figure 4**). Bare MSNPs without any modifications were used as the control. The percentage weight loss of bare MSNPs was about 5.3% over the whole temperature range, which was largely due to the removal of absorbed water and the dehydroxylation of

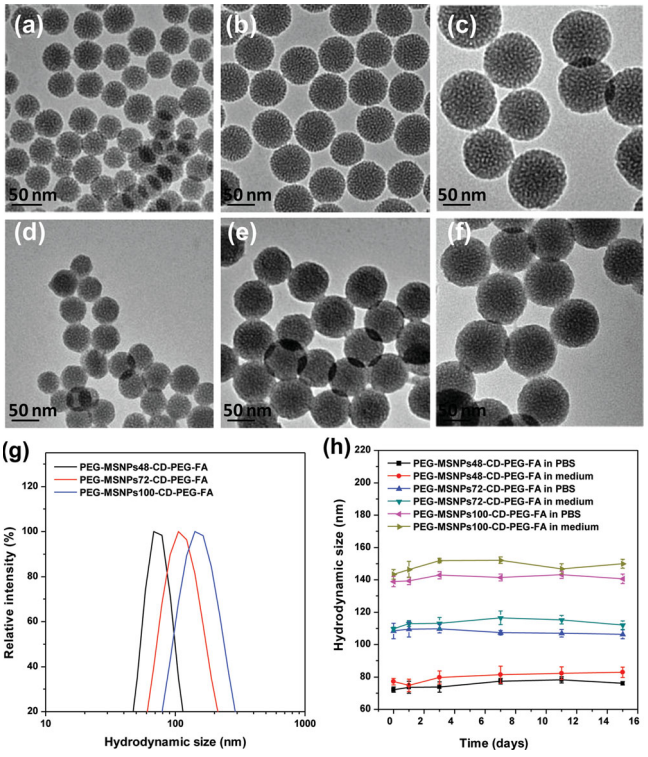

Figure 3. a–f) TEM images of a–c) PEG-MSNPs-SS-CD and d–f) PEG-MSNPs-CD-PEG-FA with different sizes of a,d) 48 nm, b,e) 72 nm, and c,f) 100 nm. g) Hydrodynamic size distributions of different-sized PEG-MSNPs-CD-PEG-FA in PBS buffer solution (pH 7.4). h) Long-term colloidal stability of different-sized PEG-MSNPs-CD-PEG-FA in PBS (pH 7.4) or culture medium containing 10% FBS. The error bars were obtained from three independent measurements.

© 2013 WILEY-VCH Verlag GmbH & Co. KGaA, Weinheim

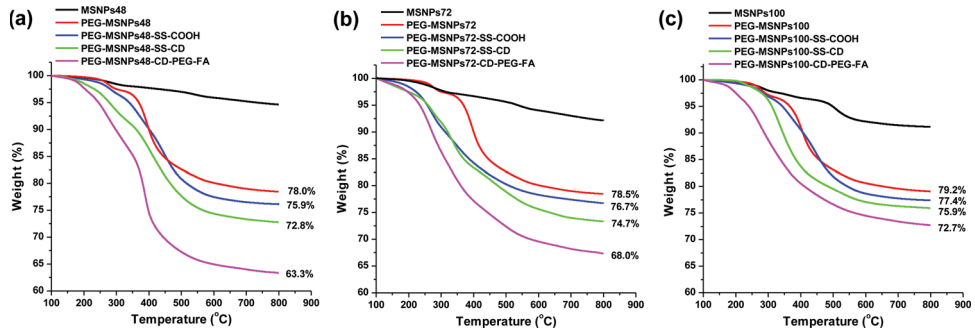

Figure 4. TGA curves of bare MSNPs, PEG-MSNPs, PEG-MSNPs-SS-COOH, PEG-MSNPs-SS-CD, and PEG-MSNPs-CD-PEG-FA with different sizes of a) 48 nm, b) 72 nm, and c) 100 nm.

silanol groups. For PEG-MSNPs, the percentage weight loss was significant, because low molecular weight PEG chains were degraded at ≈280 °C.[59] Moreover, greater weight losses of PEG-MSNPs-SS-COOH, PEG-MSNPs-SS-CD and PEG-MSNPs-CD-PEG-FA were attributed to the degradation of β-CD$(NH_2)_7$ and FA-PEG-Ad, indicating that β-CD$(NH_2)_7$ and FA-PEG-Ad were successfully immobilized onto the surface of the nanoparticles. Quantitative analysis of the β-CD$(NH_2)_7$ and FA-PEG-Ad units in PEG-MSNPs-CD-PEG-FA was carried out based on the percentage weight loss in the TGA curve. The weight losses of PEG-MSNPs48-SS-COOH, PEG-MSNPs48-SS-CD, and PEG-MSNPs48-CD-PEG-FA from 100 to 800 °C were 75.9%, 72.8%, and 63.3%, respectively. Thus, the weight percentages of β-CD$(NH_2)_7$ and FA-PEG-Ad in PEG-MSNPs48-CD-PEG-FA were estimated to be about 3.1% and 9.5%, respectively. The molar ratio of β-CD$(NH_2)_7$ to FA-PEG-Ad in PEG-MSNPs48-CD-PEG-FA was calculated to be 1.23 : 1 through the equation: (weight percentage of β-CD$(NH_2)_7$/molecular weight of β-CD$(NH_2)_7$): (weight percentage of FA-PEG-Ad/ molecular weight of FA-PEG-Ad) = (3.1%/1427) : (9.5%/5413). As the density of amorphous silicate is 2.2 g cm^{-3}, it could be estimated that average 769 β-CD$(NH_2)_7$ molecules were immobilized onto one PEG-MSNPs48-SS-COOH nanoparticle (Table S2 in the Supporting Information). The mean number of the FA molecules per one PEG-MSNPs48-CD-PEG-FA nanoparticle was estimated to be 625. Similarly, the mean number of the FA molecules per PEG-MSNPs72-CD-PEG-FA and PEG-MSNPs100-CD-PEG-FA nanoparticle was estimated to be 1395 and 1804, respectively. Thus, the coating of FA-PEG-Ad on PEG-MSNPs-SS-CD nanoparticles was achieved at a molecular level.

2.2. In Vivo Biodistribution of Multifunctional MSNPs with Different Sizes

To investigate the effect of nanoparticle sizes on in vivo biodistribution of multifunctional MSNPs, MDA-MB-231 tumor-bearing Balb/c mice injected with PEG-MSNPs48-CD-PEG-FA, PEG-MSNPs72-CD-PEG-FA, or PEG-MSNPs100-CD-PEG-FA were sacrificed at 24, 48 and 72 h, respectively. Indicated major organs and tumor tissues collected from the mice were accurately weighed and then heated in 1:1:1 H_2O/HF/HNO_3 mixture solution. The obtained tissue lysates were diluted and measured by inductively coupled plasma mass spectrometry (ICP-MS) to quantify the concentration of Si element in each organ. As shown in **Figure 5**, PEG-MSNPs48-CD-PEG-FA presents the lowest Si accumulation in liver and spleen when compared with PEG-MSNPs72-CD-PEG-FA and PEG-MSNPs100-CD-PEG-FA. The time-dependent accumulation of three PEG-MSNPs-CD-PEG-FA samples in tumor was summarized in Figure 5d. The results indicate that PEG-MSNPs48-CD-PEG-FA has the highest tumor-specific uptake among the three samples and achieved the maximum

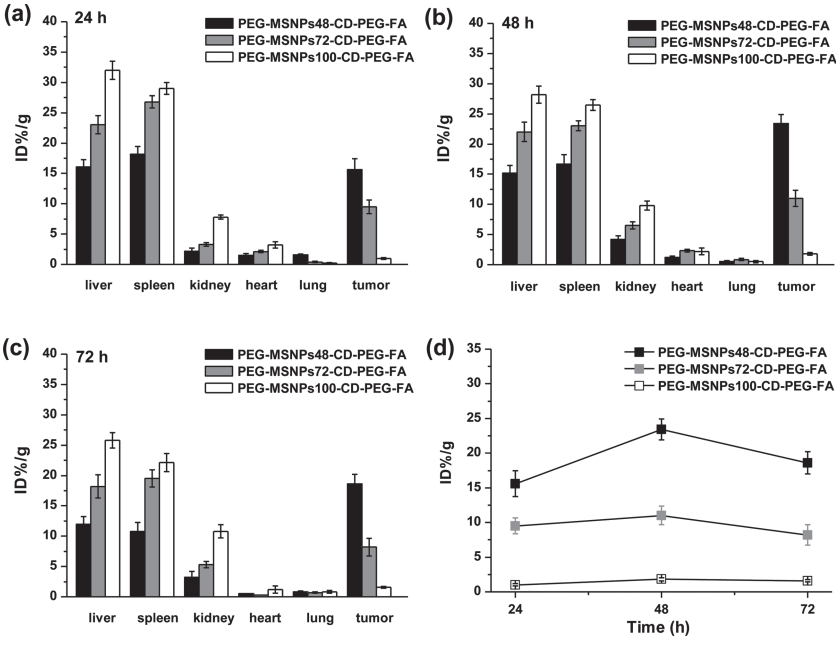

Figure 5. a–c) Biodistribution of different-sized PEG-MSNPs-CD-PEG-FA after intravenous injection into mice (dose = 20 mg kg^{-1}). The mice were sacrificed and dissected to remove tumors and major organs at different times of post injection. The Si concentrations were measured with ICP-MS and converted to the Si percentage of injected dose per gram tissue (% ID/g). The results were shown as mean values ± standard deviation (SD, n = 3). d) Time-dependent accumulation of the three PEG-MSNPs-CD-PEG-FA samples in tumors.

© 2013 WILEY-VCH Verlag GmbH & Co. KGaA, Weinheim

tumor accumulation at 48 h post-injection. PEG-MSNPs48-SS-CD coated only with mPEG-Ad that is PEG functionalized with methyl group at one end and Ad group at the other end was used as a control sample (denoted as PEG-MSNPs48-CD-PEG). In this case, Cy7.5 NHS ester, a commonly used fluorescent dye, was employed to label the amino groups of β-CD$(NH_2)_7$ in PEG-MSNPs48-CD-PEG-FA and PEG-MSNPs48-CD-PEG, respectively (Figure S4 in the Supporting Information). The treated animals were sacrificed at 72 h post-injection, and ex vivo fluorescence images were obtained for the tumor tissues and major organs. When compared with Cy7.5-labeled PEG-MSNPs48-CD-PEG (denoted as PEG-MSNPs48-CD-Cy7.5-PEG), Cy7.5-labeled PEG-MSNPs48-CD-PEG-FA (denoted as PEG-MSNPs48-CD-Cy7.5-PEG-FA) exhibits higher fluorescence intensity in the tumor tissues. This observation further confirmed the targeting role of the FA ligand on PEG-MSNPs48-CD-PEG-FA towards MDA-MB-231 breast cancer, although some PEG-MSNPs48-CD-PEG-FA nanoparticles were also detected in liver and spleen (Figure S5 in the Supporting Information). Therefore, PEG-MSNPs48-CD-PEG-FA was chosen as a suitable drug carrier for further in vitro and in vivo studies.

2.3. Drug Loading and Release Studies

To study the stimuli-triggered drug release of the PEG-MSNPs48-CD-PEG-FA carrier, Dox was first loaded into PEG-MSNPs48-SS-COOH (5 mg mL^{-1}) in solution. β-CD$(NH_2)_7$ (60 mg, 0.042 mmol) was then added to Dox-loaded PEG-MSNPs48-SS-COOH (40 mg) in the presence of 1-(3-dimethylaminopropyl)-3-ethylcarbodiimide hydrochloride (EDC·HCl, 30 mg, 0.156 mmol) in H_2O (10 mL). After the reaction mixture was stirred for 48 h, the resulting nanoparticles were collected by centrifugation, washed extensively with PBS (pH 7.4), and finally dried under vacuum. The loading percentage of Dox in PEG-MSNPs48-CD-PEG-FA determined by UV-Vis spectroscopy was ≈5%.

The drug release experiments from Dox-loaded PEG-MSNPs48-CD-PEG-FA (denoted as Dox@PEG-MSNPs48-CD-PEG-FA) were conducted at 37 °C, and 0.15 M of NaCl was used in a series of simulation solutions, that is, pH 7.4 (mimicking pH in bloodstream or extracellular fluids within normal tissues), pH 5.5 (mimicking endosomal pH inside cells), and 10 mM glutathione (mimicking GSH concentration in the cytoplasm of cancer cells). As shown in **Figure 6**, Dox@PEG-MSNPs48-CD-PEG-FA exhibits only 5.6% of drug release at pH 7.4 over a period of 48 h, indicating that the β-CD rings on the nanoparticle surface can effectively block Dox within the nanopores against the undesired drug leaching. In acidic endosomal conditions (pH 5.5), approximately 30% of Dox was released from Dox@PEG-MSNPs48-CD-PEG-FA after 48 h. It has been proved that significant release of Dox under acidic conditions is mainly attributed to the Coulombic repulsion between protonated amino groups of the β-CD$(NH_2)_7$ rings on the nanoparticle surface, leading to the opening of the nanopores and the release of positively charged Dox.[54] In addition, quick release of Dox could also be detected in the presence of GSH (10 mM) due to the removal of the β-CD capping rings via the cleavage of disulfide bonds. When the GSH concentration

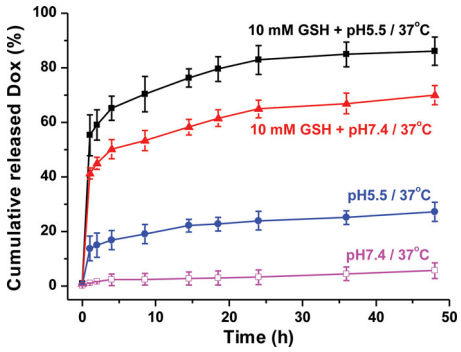

Figure 6. Release profiles of Dox@PEG-MSNPs48-CD-PEG-FA in 0.9% NaCl solution under different conditions: (□) pH 7.4, (●) pH 5.5, (▲) 10 mM GSH + pH 7.4, and (■) 10 mM GSH + pH 5.5. Data represent mean values ± SD (n = 3).

was 10 mM, approximately 42% of Dox was released in the first 1 h and up to 70% was released after 48 h, indicating an efficient release of the drug in the cytoplasm of cancer cells. The fastest release rate was achieved when the dual stimuli of pH and GSH were utilized simultaneously. In this case, about 86% of Dox was released within 48 h. These results demonstrated that Dox@PEG-MSNPs48-CD-PEG-FA, that is capable of pH- and GSH-induced intracellular drug release, is unlikely to release the entrapped drugs before entering cancerous cells, since extracellular pH is about neutral and the concentration of GSH in extracellular matrix is ~10^3 times lower than that in intracellular environment.[60,61]

2.4. Targeting Folate-Receptor Overexpressed Cancer Cells

In order to confirm the folate-mediated targeting capability of multifunctional nanoparticles, Dox@PEG-MSNPs48-CD-PEG-FA was incubated with MDA-MB-231 breast cancer cell line, which is well-known for its high over-expression of the folate receptors.[61] As shown in **Figure 7**a, red fluorescence was observed clearly in MDA-MB-231 cells after 4 h incubation with Dox@PEG-MSNPs48-CD-PEG-FA, indicating that the nanoparticles were endocytosed by the cells. After 12 h of incubation, more nanoparticles were internalized and some Dox molecules were detected in the cell nuclei, which increased significantly after 24 h. At this stage, apoptotic cell bodies were observed, on account of effective intracellular Dox release from Dox@PEG-MSNPs48-CD-PEG-FA. In contrast, there were almost no endocytosed nanoparticles observed in MDA-MB-231 cells after 4 h incubation with either Dox@PEG-MSNPs48-CD-PEG or Dox@PEG-MSNPs48-CD-PEG-FA in the presence of free FA as the competitor. After 24 h of incubation, few nanoparticles were taken up into MDA-MB-231 cells possibly via non-specific endocytosis, and very small amount of Dox was observed in the nuclei. These observations demonstrated that the introduction of the FA ligand could significantly improve the specific targeting of the nanoparticle carrier towards folate receptor overexpressed MDA-MB-231 cells. The observations were qualitatively confirmed by the line scanning profiles of fluorescent intensity on the selected MDA-MB-231 cells (Figure 7b–d).

© 2013 WILEY-VCH Verlag GmbH & Co. KGaA, Weinheim

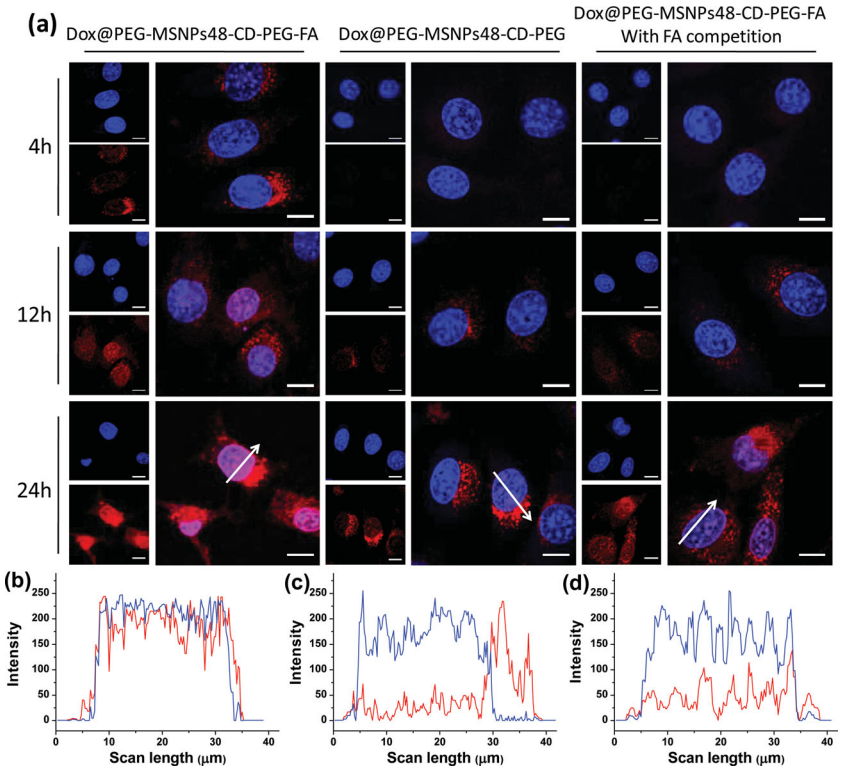

Figure 7. a) Confocal laser scanning microscopy (CLSM) images of MDA-MB-231 cancer cells incubated with Dox@PEG-MSNPs48-CD-PEG-FA, Dox@PEG-MSNPs48-CD-PEG, and Dox@PEG-MSNPs48-CD-PEG-FA under the FA competition, respectively. The red fluorescence was from Dox, and the blue fluorescence was from 4′,6-diamidino-2-phenylindole (DAPI) used to stain the nuclei. Scale bars: 20 mm. b–d) Line scanning profiles of fluorescence intensity for MDA-MB-231 cells incubated for 24 h with b) Dox@PEG-MSNPs48-CD-PEG-FA, c) Dox@PEG-MSNPs48-CD-PEG, and d) Dox@PEG-MSNPs48-CD-PEG-FA under the FA competition.

The in vitro cytotoxicity of Dox@PEG-MSNPs-CD-PEG-FA was evaluated against MDA-MB-231 breast cancer cells and MCF-10A breast normal cells (**Figure 8**). Cells were respectively treated with Dox@PEG-MSNPs48-CD-PEG-FA, Dox@PEG-MSNPs48-CD-PEG, free Dox, and empty PEG-MSNPs48-CD-PEG-FA carrier for 72 h, and the percentage of viable cells was determined by 3-(4,5-dimethylthiazol-2-yl)-5-(3-carboxymethoxyphenyl)-2-(4-sulfophenyl)-2H-tetrazolium (MTS) assay. The results reveal that PEG-MSNPs48-CD-PEG-FA was not toxic to both cell lines even at concentrations of up to 400 μg mL^{-1}. In contrast, the inhibition of breast cancer cell growth was observed when the cells were treated with Dox-loaded nanoparticles. The half-maximal inhibitory concentration (IC_{50}) of Dox@PEG-MSNPs48-CD-PEG-FA against MDA-MB-231 cells (Figure 8a) was 0.92 ± 0.21 μg mL^{-1} after 72 h of incubation, while IC_{50} of Dox@PEG-MSNPs48-CD-PEG on MDA-MB-231 cells was 3.22 ± 1.01 μg mL^{-1} at 72 h. Cytotoxic efficacy of Dox@PEG-MSNPs48-CD-PEG-FA was higher than that of Dox@PEG-MSNPs48-CD-PEG towards MDA-MB-231 cells, indicating that the targeting effect of Dox@PEG-MSNPs48-CD-PEG-FA through folate receptor-mediated endocytosis increased the internalization of the nanoparticles and thus led to a high percentage of Dox release into MDA-MB-231 cells for therapy. Moreover, significantly low cytotoxicity was observed for both Dox@PEG-MSNPs48-CD-PEG-FA (IC_{50} = 11.52 ± 1.65 μg mL^{-1}) and Dox@PEG-MSNPs48-CD-PEG (IC_{50} = 14.06 ± 1.76 μg mL^{-1}) on MCF-10A breast normal cells (Figure 8b), due to the low folate receptor expression on the cell surface. Thus, cancer cell-selective apoptosis of Dox@PEG-MSNPs48-CD-PEG-FA is attributed to the cooperative effects of folate receptor-mediated targeting as well as GSH- and pH-triggered intracellular Dox release, a mechanism which is consistent with our previous report.[55]

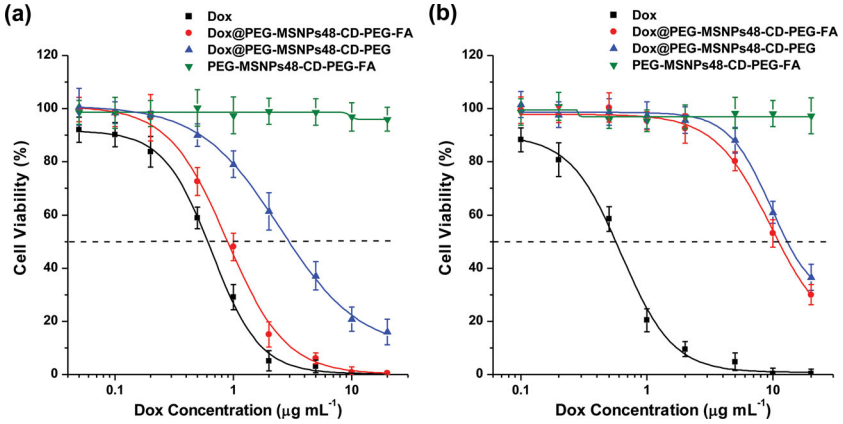

Figure 8. In vitro cytotoxicity of Dox@PEG-MSNPs48-CD-PEG-FA, Dox@PEG-MSNPs48-CD-PEG, free Dox, and empty PEG-MSNPs48-CD-PEG-FA carrier against a) MDA-MB-231 breast cancer cells and b) MCF-10A breast normal cells at different Dox doses for 72 h. The concentration of the empty PEG-MSNPs48-CD-PEG-FA carrier was equivalent to the concentration of PEG-MSNPs48-CD-PEG-FA in Dox@PEG-MSNPs48-CD-PEG-FA. Data represent mean values ± SD (n = 3).

2.5. In Vivo Antitumor Effect

The reduced toxicity and selective endocytosis of Dox@PEG-MSNPs48-CD-PEG-FA when compared with free Dox suggest that Dox@PEG-MSNPs48-CD-PEG-FA could be effective at both controlling tumor growth and reducing systemic toxicity. Hence, we evaluated the in vivo therapeutic efficacy of Dox@PEG-MSNPs48-CD-PEG-FA. Sixteen female nude mice were implanted orthotopically in the mammary fat pad with MDA-MB-231 breast carcinoma cells. Ten days after the tumor implantation, four mice groups (3, 3, 4, 4) bearing subcutaneous tumor with a mean tumor volume of 7.5 mm^3 were selected. The four groups of tumor-bearing animals were injected intravenously with Dox@PEG-MSNPs48-CD-

© 2013 WILEY-VCH Verlag GmbH & Co. KGaA, Weinheim

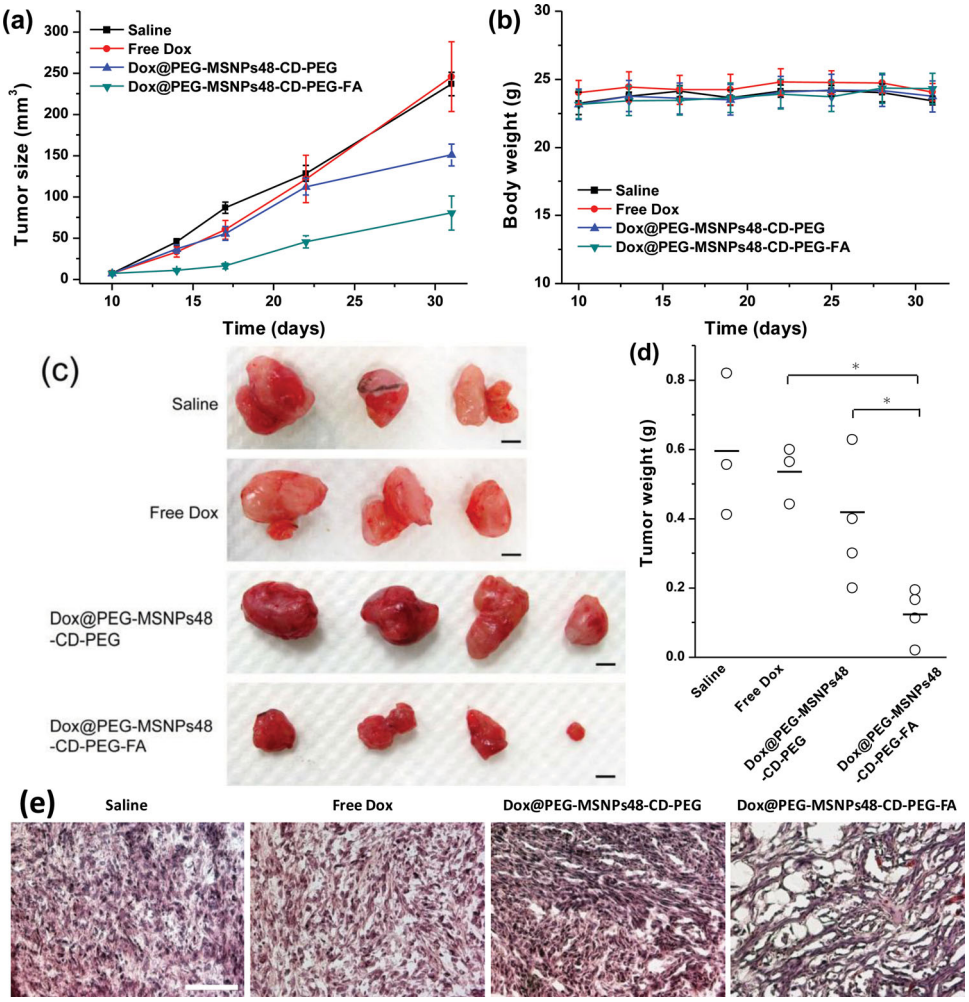

Figure 9. In vivo anticancer effect of free Dox and Dox-loaded nanoparticles injected into female nude mice. a) Tumor volume changes of different treatment groups. b) Body weight changes of MDA-MB-231 tumor bearing mice. c) Excised MDA-MB-231 solid tumors from different treatment groups at the 31st day. Scale bars: 5 mm. d) Tumor weight from different treatment groups at the 31st day. e) H&E stained MDA-MB-231 tumor sections. Nuclei were stained blue while extracellular matrix and cytoplasm were stained red. Scale bars: 100 μm.

PEG-FA (0.5 mg Dox kg^{-1}), Dox@PEG-MSNPs48-CD-PEG (0.5 mg Dox kg^{-1}), free Dox (0.5 mg Dox kg^{-1}) and saline as the control, respectively. The injections were performed thrice a week for a total of nine doses over three weeks.

Consistent with our in vitro findings, Dox@PEG-MSNPs48-CD-PEG-FA shows significantly higher rate of tumor shrinkage than Dox@PEG-MSNPs48-CD-PEG and free Dox (**Figure 9**a and Figure S6 in the Supporting Information). The treatments were well tolerated as no statistically significant body weight loss was observed in any of the treated groups (Figure 9b). At the end of the experiment, the tumor tissues were excised for accurate weighing and comparative analysis (Figure 9c). The results show a remarkable reduction (ca. 80%) in tumor weight for the four mice treated with Dox@PEG-MSNPs48-CD-PEG-FA when compared with the tumor weight (ca. 30%) of the four mice treated with Dox@PEG-MSNPs48-CD-PEG (Figure 9d). This difference was statistically significant ($p < 0.05$). In situ histological analysis also supported the excellent therapeutic effect of Dox@PEG-MSNPs48-CD-PEG-FA. When Dox@PEG-MSNPs48-CD-PEG-FA was administered, few tumor cells or foci were detected in hematoxylin and eosin (H&E) stained images (Figure 9e). In addition, H&E examinations of heart, lung, liver, spleen, and kidney indicate no apparent abnormality or lesion after 21 days post-treatment of Dox@PEG-MSNPs48-CD-PEG-FA (Figures S7–S11 in the Supporting Information). We also examined the development of clinically detectable macro-metastases connected with invasive potential of MDA-MB-231 cancer cells. The Dox@PEG-MSNPs48-CD-PEG-FA treatment prevented the macro-metastasis formation in lymphonodus in comparison to the groups of mice treated with saline and free Dox (Table S3 and Figure S12 in the Supporting Information). This effect was probably related to the decreases of subcutaneous tumor growth and of its associated neoangiogenesis, both of which delayed the spread of cancer cells and subsequent distal metastasis.

Efficient delivery of Dox into cancer cells increases the intracellular drug concentration to inhibit cell growth, ultimately leading to the cell death. To examine antitumor activity of the

© 2013 WILEY-VCH Verlag GmbH & Co. KGaA, Weinheim

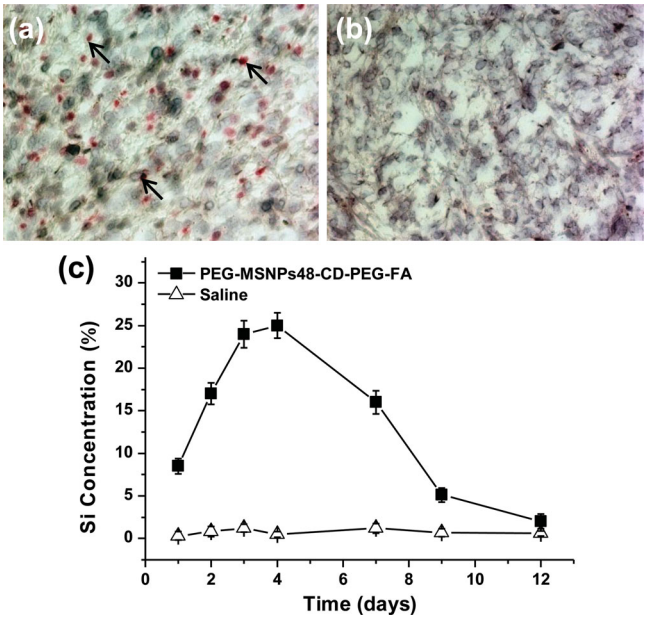

Figure 10. a,b) TUNEL assays for apoptotic cell death. The mice were sacrificed 72 h after the intravenous injection of a) Dox@PEG-MSNPs48-CD-PEG-FA (Dox 2.5 mg kg^{-1}) and b) PEG-MSNPs48-CD-PEG-FA. Tumor sections were used for TUNEL staining and visualized under a light microscope. Arrows indicated the examples of TUNEL-positive (red color) cells with apoptotic morphology. c) ICP-MS analysis of the Si concentration in urine and feces of mice injected with PEG-MSNPs48-CD-PEG-FA (MSNP-treated group) or saline (control group). The numbers shown are the average percentages of the Si concentrations detected in urine and feces compared to the total injection amount of PEG-MSNPs48-CD-PEG-FA (1 mg). Data represent mean values ± SD (n = 3).

drug, apoptotic cells in tumor tissues were evaluated using terminal deoxynucleotidyl transferase-mediated-dUTP nick-end labeling (TUNEL) assay. TUNEL-positive tumor cell nuclei (red color) were detected in tumor tissues of the mice treated with Dox@PEG-MSNPs48-CD-PEG-FA (**Figure 10**a), whereas apoptotic cells were rarely detectable when treated with empty PEG-MSNPs48-CD-PEG-FA carrier (Figure 10b). These results demonstrated that Dox from Dox@PEG-MSNPs48-CD-PEG-FA was successfully delivered to the tumor sites, and its antitumor activity was retained.

Potential in vivo toxicity is always a great concern for nanomaterial-based drug carriers used in biomedicine. Since mice treated with multifunctional MSNPs appeared normal under the current experimental conditions, we proposed that the injected PEG-MSNPs48-CD-PEG-FA might be excreted from the animal body. To test this hypothesis, we measured the Si concentrations in urine and feces collected from the mice after injection of PEG-MSNPs48-CD-PEG-FA at different time points. The concentration of PEG-MSNPs48-CD-PEG-FA in urine and feces, evaluated by ICP-MS, was maximal at 3–4 days after the injection, and the cumulative amount of excreted Si reached 92% of the injected Si after 12 days (Figure 10c). These results demonstrated that most of the administered PEG-MSNPs48-CD-PEG-FA could be excreted from the animal body, which further explained the low toxicity of the nanoparticle carrier observed in the biocompatibility experiments.

3. Conclusions

In summary, we have synthesized PEG-MSNPs-CD-PEG-FA with three different sizes (48, 72, and 100 nm) for cancer-targeted drug delivery in vivo, and have demonstrated that PEG-MSNPs-CD-PEG-FA with a core diameter of 48 nm exhibits high accumulation in tumor tissues and specific targeting for MDA-MB-231 cancer cells. Furthermore, in vivo investigation of therapeutic efficacy has been successfully carried out, indicating that PEG-MSNPs48-CD-PEG-FA could deliver sufficient amount of Dox into tumor, resulting in a remarkable tumor-inhibiting effect compared with those of free Dox and non-targeted nanoparticles. After the drug delivery, most of the administered PEG-MSNPs48-CD-PEG-FA could be excreted from the animal body. These results demonstrate that PEG-MSNPs48-CD-PEG-FA is an efficient carrier for targeted drug delivery to folate receptor-overexpressed cancer cells in tumor tissues. Biocompatible, uniform, redispersible and fluorescence-labeled PEG-MSNPs48-CD-PEG-FA carrier is a promising candidate for simultaneous optical imaging and anticancer drug delivery in cancer diagnostics and treatment.

4. Experimental Section

Materials: Cetyltrimethylammonium chloride (CTAC, 25 wt%), doxorubicin hydrochloride (Dox·HCl), folic acid (FA), tetraethylorthosilicate (TEOS), and triethanolamine (TEA) were purchased from Sigma-Aldrich. β-Cyclodextrin (β-CD), 1-(3-dimethylaminopropyl)-3-ethylcarbodiimide hydrochloride (EDC·HCl), glutathione (GSH), and 3-mercaptopropyltrimethoxysilane (MPTMS) were purchased from Alfa Aesar. PEG-silane (MW 575–750 g mol^{-1}, 50% in ethanol) was obtained from Gelest (Morrisville, PA). β-CD$(NH_2)_7$ was synthesized as described previously.[44] mPEG-Ad (MW 5173.23) and FA-PEG-Ad (MW 5413.38) were synthesized according to our previously reported methods.[55] 2-Carboxyethyl-2-pyridyl disulfide was synthesized according to a reported procedure.[63] 4′,6-Diamidino-2-phenylindole (DAPI), dulbecco's modified eagle's medium (DMEM), fetal bovine serum (FBS), and RPMI 1640 without phenol red were purchased from Invitrogen (Carlsbad, USA). Nanopure water (18.2 MΩ; Millipore Co., USA) was used in all experiments. All other chemicals were commercially available and used as received unless otherwise stated.

Characterizations: ^{1}H NMR spectra were recorded on a Bruker BBFO-400 spectrometer. TEM images were collected on a JEOL JEM-1400 instrument operated at an acceleration voltage of 100 kV. TEM samples were prepared by pipetting a drop of nanoparticle solution onto 200-mesh copper grid coated with carbon, and the grid was dried under air before the measurement. UV-Vis spectra were carried out on a Shimadzu UV-3600 UV-Vis-NIR spectrometer. Fluorescence spectra were recorded on a Cary Eclipse Fluorescence spectrophotometer. FT-IR spectra were recorded as KBr-pellet on a Perkin-Elmer 1760X FT-IR spectrometer. Nitrogen adsorption/desorption isotherms were measured on a Quantachrome Instruments Autosorb-iQ (Boynton Beach, Florida USA) with the extra-high pure gases. The samples were degassed at 120 °C for 3 h. The surface areas were calculated by the Brunauer-Emmett-Teller (BET) method, and pore size was calculated from desorption branches of isotherms by the Barrett-Joyner-Halenda (BJH) method. Dynamic light scattering (DLS) and zeta potential experiments were performed at 25 °C using a Malvern Zetasizer NanoZS instrument. All of the measurements were performed with the nanoparticles suspended

© 2013 WILEY-VCH Verlag GmbH & Co. KGaA, Weinheim

in filtered water or filtered cell culture media at a concentration of 50 μg mL^{-1}. The data were analyzed by Malvern Dispersion Technology Software. Thermogravimetric analysis (TGA) was carried out for powder samples using a TGA Q500 recorded from 100 to 800 °C in airflow at a heating rate of 10 °C min^{-1}.

Synthesis of Different-Sized PEG-MSNPs: CTAC (2 g, 25 wt%) and TEA (80 mg) were dissolved in distilled H_2O (20 mL) under vigorous stirring. The mixture reaction was heated to 95 °C. TEOS (1.5 mL) was then added to the solution. After 10 min, PEG-silane (1 mL) was added in four equal potions every three minutes. This step was followed by stirring at 95 °C for 30 min. After the reaction mixture was cooled down to room temperature, the nanoparticles were collected by centrifugation, and washed several times with ethanol. In order to remove surfactant template (CTAC) from the mesopores of the nanoparticles, the as-synthesized nanoparticles were suspended in a mixture of ethanol (12 mL) and concentrated HCl (1 mL, 37%), and the solution was treated three times by sonication in an ice bath for 30 min. Finally, the surfactant-removed PEG-MSNPs48 was obtained by washing several times with ethanol, and drying the nanoparticles from ethanolic suspensions using evaporation. For the synthesis of PEG-MSNPs72 and PEG-MSNPs100, the synthetic procedure was similar to that of PEG-MSNPs48. The differences were changing TEA concentrations to be 2.5 and 1 mg mL^{-1}, respectively. In addition, PEG-silane was added at 20 and 30 minutes, respectively.

Synthesis of PEG-MSNPs-SS-COOH: PEG-MSNPs (100 mg) were suspended in anhydrous toluene (20 mL), and MPTMS (1 mL) was added to the solution. The mixture solution was heated to 80 °C and stirred under N_2 for 6 h. After centrifugation and washing with toluene and ethanol, sulphydryl-functionalized PEG-MSNPs were treated with a solution of 2-carboxyethyl-2-pyridyl disulfide (100 mg, 0.46 mmol) in ethanol (5 mL) at room temperature under vigorous stirring for 48 h. The resulting PEG-MSNPs-SS-COOH was separated by centrifugation, washed with ethanol, and dried under vacuum.

Drug Loading: Dox loading was performed according to our previous study.[55] Firstly, PEG-MSNPs48-SS-COOH (40 mg) was dispersed into anhydrous DMF solution (2 mL) containing Dox (5 mg mL^{-1}). After the mixture solution was stirred overnight, it was sonicated to maximize the nanoparticle dispersion. Dox-loaded PEG-MSNPs48-SS-COOH was obtained by centrifugation. β-CD$(NH_2)_7$ (60 mg, 0.042 mmol) was then added to an aqueous solution (10 mL) containing Dox-loaded PEG-MSNPs48-SS-COOH in the presence of EDC·HCl (30 mg, 0.156 mmol). After the mixture solution was stirred for 48 h, the resulting nanoparticles were collected by centrifugation, and washed extensively with PBS buffer (pH 7.4). The loading percentage of Dox in PEG-MSNPs48-SS-CD was estimated through the UV-Vis absorption measurements by subtracting the amount of Dox in the collected supernatant from the total amount of Dox added. For surface modification with FA-PEG-Ad, Dox-loaded PEG-MSNPs48-SS-CD (20 mg) was suspended in PBS buffer (5 mL, pH 7.4), and then FA-PEG-Ad (100 mg) was added to the suspension. The mixture was stirred at room temperature for 12 h. Dox-loaded PEG-MSNPs48-CD-PEG-FA was obtained by centrifugation, and washed several times with PBS (pH 7.4). The product was donated as Dox@PEG-MSNPs48-CD-PEG-FA. For surface modification with mPEG-Ad, Dox-loaded PEG-MSNPs48-SS-CD (20 mg) and mPEG-Ad (100 mg) were stirred in PBS buffer (5 mL, pH 7.4) for 12 h. Dox-loaded PEG-MSNPs48-CD-PEG was collected by centrifugation, and washed with PBS (pH 7.4). The product was donated as Dox@PEG-MSNPs48-CD-PEG.

Drug Release: To determine the kinetics of Dox release from the nanoparticles, a Dox@PEG-MSNPs48-CD-PEG-FA suspension (3 mL, 1 mg mL^{-1}) was dialyzed (MWCO 14000) against phosphate buffer (10 mM phosphate, 50 mL) with 0.9% NaCl at 37 °C under different conditions: pH 7.4, pH 5.5, 10 mM GSH with pH 7.4, and 10 mM GSH with pH 5.5. At different times, the Dox concentration in the outside solution was calculated by comparing fluorescence intensity at 593 nm (λ_{ex} = 480 nm) with reference to the standard curve.

Cell Culture: MDA-MB-231 breast cancer cells were cultured in DMEM containing 10% FBS, penicillin (100 U mL^{-1}), streptomycin (100 μg mL^{-1}), and *L*-glutamine (2 mM) in a humidified atmosphere with 5% CO_2 at 37 °C. MCF-10A breast epithelial cells were cultured in DMEM/F12 (Invitrogen, 11330–032) supplemented with 5% horse serum (Invitrogen, 16050–122), 1% penicillin/streptomycin (Invitrogen, 15070–063), hydrocortisone (0.5 μg mL^{-1}, Sigma, H-0888), cholera toxin (100 ng mL^{-1}, Sigma, C-8052), insulin (10 μg mL^{-1}, Sigma, I-1882), and recombinant human EGF (20 ng mL^{-1}, Peprotech, 100–15). The medium was routinely changed every 3 days and the cells were separated by trypsinization before reaching the confluence.

Confocal Laser Scanning Microscopy (CLSM): The MDA-MB-231 cells were treated with Dox@PEG-MSNPs48-CD-PEG-FA (50 μg mL^{-1}) or Dox@PEG-MSNPs48-CD-PEG (50 μg mL^{-1}) in the culture medium at 37 °C for 4, 12 and 24 h, respectively. For free FA competition experiments, the cells were cultured with FA (1 mM) for 24 h prior to the addition of the nanoparticles. The cells were washed three times with PBS and fixed with fresh 4.0% formaldehyde at room temperature for 15 min. After washing with PBS, the cells were stained with DAPI (1 μg mL^{-1}) for 15 min. The images were taken using a Nikon laser-scanning confocal A1 microscope (100× oil objective, 405/488 nm excitation).

Cell Growth Inhibition Assay: The cells were seeded into 96-well plate at a density of 5×10^3 cells per well in complete DMEM medium (200 μL), and then incubated in a humidified 5% CO_2 atmosphere at 37 °C for 24 h. The culture medium was then replaced with fresh culture medium (200 μL) containing either free Dox or Dox-loaded nanoparticles at different Dox doses. The cells were further incubated for 72 h, and then washed three times with PBS in order to remove free Dox or nanoparticles. A portion (20 μL) of 3-(4,5-dimethylthiazol-2-yl)-5-(3-carboxymethoxyphenyl)-2-(4-sulfophenyl)-2H-tetrazolium (MTS)/phenazinemethosulfate (PMS) solution (20:1, v/v, CellTiter 96 AQueous kit) was added to each well of a 96-well plate containing cells in RPMI 1640 (100 μL) without phenol red. After incubation in a humidified 5% CO_2 atmosphere at 37 °C for 1 h, the absorbance at 490 nm was recorded using a microplate reader (infinite M200, TECAN). The spectrophotometer was calibrated to zero absorbance by using culture medium without cells. The relative cell viability compared to control wells containing medium without Dox or nanoparticles was calculated by $[A]_{test}/[A]_{control}$, where $[A]_{test}$ and $[A]_{control}$ are the average absorbance of the test and control samples, respectively. The IC_{50} values were calculated using GraphPad Prism software (version 5.01), which were based on three independent experiments.

Human Cancer Xenograph Establishment: Balb/c nude female mice were purchased from the Jackson laboratory (Bar Harbor, Maine). All animal experiments were conducted under protocols approved by the Animal Care and Use Committee of Nanyang Technological University. The adherent MDA-MB-231 tumor cells were washed with PBS, harvested from confluent culture by 3-minutes exposure to 0.25% trypsin in an incubator. Trypsinization was stopped with a medium containing 10% FBS. The cells were centrifuged at 100 g under 4 °C for 4 min, and the floating cells in the supernatant were discarded. The cell pellet was re-suspended in a medium contain 10% FBS and then mixed thoroughly. The re-suspended cells with dilutions of 3×10^6 per 100 μL in a cell growth medium and 30% matrigel (BD Biosciences, Bedford, MA) were injected subcutaneously into right flank area of each mouse.

In Vivo Therapeutic Efficacy: Mice were injected via the tail vein with i) saline, ii) free Dox (1.5 mg kg^{-1} week^{-1}), iii) Dox@PEG-MSNPs48-CD-PEG (30 mg kg^{-1} week^{-1}), and iv) Dox@PEG-MSNPs48-CD-PEG-FA (30 mg kg^{-1} week^{-1}), respectively. Mammary tumors were measured thrice weekly using a caliper, and tumor volume was calculated using the formula $V_{tumor} = a \times (b^2/2)$, where a is the maximum length and b is the minimal width. All mice were sacrificed by exposure to carbon dioxide, dissected organ and tumor tissues of sacrificed mice were fixed in 4% paraformaldehyde and processed routinely into paraffin, sectioned at 5 μm, and stained with hematoxylin and eosin (H&E) procedure. Examined tissues included: tumor, liver, spleen, kidney, heart, and lung.

TUNEL Assay: Tumors arising from MDA-MB-231 subcutaneously transplanted nude mice were excised, weighed, sectioned and assessed for apoptosis by the terminal deoxynucleotidyl transferase-mediated-dUTP nick-end labeling (TUNEL) assay according to the instructions of a commercial kit (In Situ Cell Death Detection Kit, AP; Roche). Tissue

© 2013 WILEY-VCH Verlag GmbH & Co. KGaA, Weinheim

sections were stained with TUNEL, and AP red was used for visualization of immunostaining, with cells stained as red considered to be TUNEL positive. Blue color was from hematoxylin counterstaining in order to visualize all cellular nuclei. Representative pictures were presented (20× magnification). The tissues were immunostained with the addition of secondary anti-FITC-AP conjugate and AP red. The counterstaining was performed with hematoxylin (with blue color) for visualization of all cellular nuclei. Histological sections were evaluated using light microscopy (Leica Qwin).

Statistical Analysis: Data were collected from three or more replicates for each experiment, and they were presented as mean ± standard deviation (SD). Statistical significance was determined using Student's *t*-test. A *p*-value less than 0.05 was considered statistically significant.

Supporting Information

Supporting Information is available from the Wiley Online Library or from the author.

Acknowledgements

Q.Z. and X.W. contributed equally to this work. This work was financially supported by the Singapore National Research Foundation Fellowship (NRF2009NRF-RF001–015), the Singapore National Research Foundation CREATE program – Singapore Peking University Research Centre for a Sustainable Low-Carbon Future, and the NTU-A*Star Centre of Excellence for Silicon Technologies (A*Star SERC No.: 112 351 0003).

Received: August 27, 2013
Revised: November 10, 2013
Published online: December 21, 2013

[1] M. Ferrai, *Nat. Rev. Cancer* **2005**, *5*, 161–171.
[2] D. Peer, J. M. Karp, S. Hong, O. C. Farokhzad, R. Margalit, R. Langer, *Nat. Nanotechnol.* **2007**, *2*, 751–760.
[3] N. L. Rosi, C. A. Mirkin, *Chem. Rev.* **2005**, *105*, 1547–1562.
[4] I. L. Medintz, H. T. Uyeda, E. R. Goldman, H. Mattoussi, *Nat. Mater.* **2005**, *4*, 435–446.
[5] M. E. Davis, Z. Chen, D. M. Shin, *Nat. Rev. Drug Discovery* **2008**, *7*, 771–782.
[6] V. P. Torchilin, *Nat. Rev. Drug Discovery* **2005**, *4*, 145–160.
[7] R. Xie, S. Hong, L. Feng, J. Rong, X. Chen, *J. Am. Chem. Soc.* **2012**, *134*, 9914–9917.
[8] W. T. Al-Jamal, K. Kostarelos, *Acc. Chem. Res.* **2011**, *44*, 1094–1104.
[9] S.-M. Lee, H. Chen, C. M. Dettmer, T. V. OHalloran, S. T. Nguyen, *J. Am. Chem. Soc.* **2007**, *129*, 15096–15097.
[10] N. Doshi, S. Mitragotri, *Adv. Funct. Mater.* **2009**, *19*, 3843–3854.
[11] N. Kamaly, Z. Xiao, P. M. Valencia, A. F. Radovic-Moreno, O. C. Farokhzad, *Chem. Soc. Rev.* **2012**, *41*, 2971–3010.
[12] E. R. Gillies, J. M. J. Fréchet, *Drug Discovery Today* **2005**, *10*, 35–43.
[13] J. E. Lee, N. Lee, H. Kim, J. Kim, S. H. Choi, J. H. Kim, T. Kim, I. C. Song, S. P. Park, W. K. Moon, T. Hyeon, *J. Am. Chem. Soc.* **2010**, *132*, 552–557.
[14] B. P. Bastakoti, Y.-C. Hsu, S.-H. Liao, K. C.-W. Wu, M. Inoue, S. Yusa, K. Nakashima, Y. Yamauchi, *Chem. Asian J.* **2013**, *8*, 1301–1305.
[15] F. Zhang, G. B. Braun, A. Pallaoro, Y. Zhang, Y. Shi, D. Cui, M. Moskovits, D. Zhao, G. D. Stucky, *Nano Lett.* **2012**, *12*, 61–67.
[16] D.-W. Wang, X.-M. Zhu, S.-F. Lee, H.-M. Chan, H.-W. Li, S. K. Kong, J. C. Yu, C. H. K. Cheng, Y.-X. J. Wang, K. C.-F. Leung, *J. Mater. Chem. B* **2013**, *1*, 2934–2942.
[17] H. Meng, M. Xue, T. Xia, Z. Ji, D. Y. Tarn, J. I. Zink, A. E. Nel, *ACS Nano* **2011**, *5*, 4131–4144.
[18] Q. He, Z. Zhang, F. Gao, Y. Li, J. Shi, *Small* **2011**, *7*, 271–280.
[19] H. Maeda, J. Wu, T. Sawa, Y. Matsumura, K. Hori, *J. Controlled Release* **2000**, *65*, 271–284.
[20] M. M. Gottesman, T. Fojo, S. E. Bates, *Nat. Rev. Cancer* **2002**, *2*, 48–58.
[21] D. Schrama, R. A. Reisfeld, J. C. Becker, *Nat. Rev. Drug Discovery* **2006**, *5*, 147–159.
[22] J. D. Byrne, T. Betancourt, L. Brannon-Peppas, *Adv. Drug Delivery Rev.* **2008**, *60*, 1615–1626.
[23] A. Schroeder, D. A. Heller, M. M. Winslow, J. E. Dahlman, G. W. Pratt, R. Langer, T. Jacks, D. G. Anderson, *Nat. Rev. Cancer* **2012**, *12*, 39–50.
[24] M. W. Ambrogio, C. R. Thomas, Y. L. Zhao, J. I. Zink, J. F. Stoddart, *Acc. Chem. Res.* **2011**, *44*, 903–913.
[25] J. L. Vivero-Escoto, I. I. Slowing, B. G. Trewyn, V. S.-Y. Lin, *Small* **2010**, *6*, 1952–1967.
[26] J. M. Rosenholm, C. Sahlgren, M. Lindén, *Nanoscale* **2010**, *2*, 1870–1883.
[27] F. Tang, L. Li, D. Chen, *Adv. Mater.* **2012**, *24*, 1504–1534.
[28] Z. Li, J. C. Barnes, A. Bosoy, J. F. Stoddart, J. I. Zink, *Chem. Soc. Rev.* **2012**, *41*, 2590–2605.
[29] Y. Chen, H. Chen, J. Shi, *Adv. Mater.* **2013**, *25*, 3144–3176.
[30] D. R. Radu, C.-Y. Lai, K. Jeftinija, E. W. Rowe, S. Jeftinija, V. S.-Y. Lin, *J. Am. Chem. Soc.* **2004**, *126*, 13216–13217.
[31] S. Giri, B. G. Trewyn, M. P. Stellmaker, V. S.-Y. Lin, *Angew. Chem. Int. Ed.* **2005**, *44*, 5038–5044.
[32] T. D. Nguyen, Y. Liu, S. Saha, K. C.-F. Leung, J. F. Stoddart, J. I. Zink, *J. Am. Chem. Soc.* **2007**, *129*, 626–634.
[33] J. L. Vivero-Escoto, I. I. Slowing, C.-W. Wu, V. S.-Y. Lin, *J. Am. Chem. Soc.* **2009**, *131*, 3462–3463.
[34] S. Angelos, Y.-W. Yang, K. Patel, J. F. Stoddart, J. I. Zink, *Angew. Chem. Int. Ed.* **2008**, *47*, 2222–2226.
[35] E. Climent, R. Martínez-Máñez, F. Sancenón, M. D. Marcos, J. Soto, A. Maquieira, P. Amorós, *Angew. Chem. Int. Ed.* **2010**, *49*, 7281–7283.
[36] Y. Zhao, J. L. Vivero-Escoto, I. I. Slowing, B. G. Trewyn, V. S.-Y. Lin, *Expert Opin. Drug Delivery* **2010**, *7*, 1013–1029.
[37] D. Li, J. Tang, C. Wei, J. Guo, S. Wang, D. Chaudhary, C. Wang, *Small* **2012**, *8*, 2690–2697.
[38] C.-L. Zhu, C.-H. Lu, X.-Y. Song, H.-H. Yang, X.-R. Wang, *J. Am. Chem. Soc.* **2011**, *133*, 1278–1281.
[39] Z. Luo, K. Cai, Y. Hu, L. Zhao, P. Liu, L. Duan, W. Yang, *Angew. Chem. Int. Ed.* **2011**, *50*, 640–643.
[40] R. Liu, X. Zhao, T. Wu, P. Feng, *J. Am. Chem. Soc.* **2008**, *130*, 14418–14419.
[41] H. Kim, S. Kim, C. Park, H. Lee, H. J. Park, C. Kim, *Adv. Mater.* **2010**, *22*, 4280–4283.
[42] C. Wang, Z. Li, D. Cao, Y. L. Zhao, J. W. Gaines, O. A. Bozdemir, M. W. Ambrogio, M. Frasconi, Y. Y. Botros, J. I. Zink, J. F. Stoddart, *Angew. Chem. Int. Ed.* **2012**, *51*, 5460–5465.
[43] L. Du, S. Liao, H. A. Khatib, J. F. Stoddart, J. I. Zink, *J. Am. Chem. Soc.* **2009**, *131*, 15136–15142.
[44] Y. L. Zhao, Z. Li, S. Kabehie, Y. Y. Botros, J. F. Stoddart, J. I. Zink, *J. Am. Chem. Soc.* **2010**, *132*, 13016–13025.
[45] H. Meng, M. Xue, T. Xia, Y. L. Zhao, F. Tamanoi, J. F. Stoddart, J. I. Zink, A. E. Nel, *J. Am. Chem. Soc.* **2010**, *132*, 12690–12697.
[46] C. Park, H. Kim, S. Kim, C. Kim, *J. Am. Chem. Soc.* **2009**, *131*, 16614–16615.
[47] K. Patel, S. Angelos, W. R. Dichtel, A. Coskun, Y.-W. Yang, J. I. Zink, J. F. Stoddart, *J. Am. Chem. Soc.* **2008**, *130*, 2382–2383.
[48] C. Park, K. Lee, C. Kim, *Angew. Chem. Int. Ed.* **2009**, *48*, 1275–1278.

© 2013 WILEY-VCH Verlag GmbH & Co. KGaA, Weinheim

[49] H. Yan, C. Teh, S. Sreejith, L. Zhu, A. Kwok, W. Fang, X. Ma, K. T. Nguyen, V. Korzh, Y. L. Zhao, *Angew. Chem. Int. Ed.* **2012**, *51*, 8373–8377.
[50] B. G. Trewyn, S. Giri, I. I. Slowing, V. S.-Y. Lin, *Chem. Commun.* **2007**, 3236–3245.
[51] Y.-S. Lin, N. Abadeer, K. R. Hurley, C. L. Haynes, *J. Am. Chem. Soc.* **2011**, *133*, 20444–20457.
[52] Y.-S. Lin, N. Abadeer, C. L. Haynes, *Chem. Commun.* **2011**, *47*, 532–534.
[53] B. Haley, E. Frenkel, *Urol. Oncol.: Semin. Orig. Invest.* **2008**, *26*, 57–64.
[54] F. Alexis, E. Pridgen, L. K. Molnar, O. C. Farokhzad, *Mol. Pharm.* **2008**, *5*, 505–515.
[55] Q. Zhang, F. Liu, K. T. Nguyen, X. Ma, X. Wang, B. Xing, Y. L. Zhao, *Adv. Funct. Mater.* **2012**, *22*, 5144–5156.
[56] S.-H. Wu, C.-Y. Mou, H.-P. Lin, *Chem. Soc. Rev.* **2013**, *42*, 3862–3875.
[57] K. Möller, J. Kobler, T. Bein, *Adv. Funct. Mater.* **2007**, *17*, 605–612.
[58] J. Kobler, K. Möller, T. Bein, *ACS Nano* **2008**, *2*, 791–799.
[59] Q. Zhang, C. Wang, L. Qiao, H. Yan, K. Liu, *J. Mater. Chem.* **2009**, *19*, 8393–8402.
[60] G. Saito, J. A. Swanson, K. D. Lee, *Adv. Drug Delivery Rev.* **2003**, *55*, 199–215.
[61] A. Gupte, R. J. Mumper, *Cancer Treat. Rev.* **2009**, *35*, 32–46.
[62] R. Meier, T. D. Henning, S. Boddington, S. Tavri, S. Arora, G. Piontek, M. Rudelius, C. Corot, H. E. Daldrup-Link, *Radiology* **2010**, *255*, 527–535.
[63] J. Carlsson, H. Drevin, R. Axén, *Biochem. J.* **1978**, *173*, 723–737.

© 2013 WILEY-VCH Verlag GmbH & Co. KGaA, Weinheim